Experimental Eye Research 190 (2020) 107866

Contents lists available at ScienceDirect

Experimental Eye Research

journal homepage: www.elsevier.com/locate/yexer

Chromatic pupillometry for the characterization of the pupillary light reflex in *Octodon degus*

Nicolas Palanca-Castan*, Paloma A. Harcha, David Neira, Adrian G. Palacios

Centro Interdisciplinario de Neurociencia de Valparaiso, Universidad de Valparaiso, Gran Bretaña 1111, Valparaiso, Chile

ARTICLE INFO

Keywords:
Melanopsin
Neurodegeneration
Pupillometry
Degu

ABSTRACT

The common degu (*Octodon degus*) is an emerging model in biomedical science research due to its longevity and propensity to develop human-like conditions. However, there is a lack of standardized techniques for this non-traditional laboratory animal. In an effort to characterize the model, we developed a chromatic pupillometry setup and analysis protocol to characterize the pupillary light reflex (PLR) in our animals. The PLR is a biomarker to detect early signs for central nervous system deterioration. Chromatic pupillometry is a non-invasive and anesthesia-free method that can evaluate different aspects of the PLR, including the response of intrinsically photosensitive retinal ganglion cells (ipRGCs), the disfunction of which has been linked to various disorders. We studied the PLR of 12 degus between 6 and 48 months of age to characterize responses to LEDs of 390, 450, 500, 525 and 605 nm, and used 5 with overall better responses to establish a benchmark for healthy PLR (PLR+) and deteriorated PLR (PLR-). Degu pupils contracted up to 65% of their horizontal resting size before reaching saturation. The highest sensitivity was found at 500 nm, with similar sensitivities at lower tested intensities for 390 nm, coinciding with the medium wavelength and short wavelength cones of the degu. We also tested the post-illumination pupillary response (PIPR), which is driven exclusively by ipRGCs. PIPR was largest in response to 450 nm light, with the pupil preserving 48% of its maximum constriction 9 s after the stimulus, in contrast with 24% preserved in response to 525 nm, response driven mainly by cones. PLR- animals showed maximum constriction between 40% and 50% smaller than PLR+, and their PIPR almost disappeared, pointing to a disfunction of the iPRGCs rather than the retinal photoreceptors. Our method thus allows us to non-invasively estimate the condition of experimental animals before attempting other procedures.

1. Introduction

Octodon degus, or degu, is a hystricomorph rodent endemic to central Chile with growing interest as an animal model (for an overview, see Ardiles et al., 2013; Hurley et al., 2018). One of their more salient characteristics is their longevity. Degus can live up to 8 years in captivity (Lee, 2004), which makes them good candidates for studies on the effects of aging and the associated plethora of degenerative and metabolic disorders like diabetes, amyloidosis and atherosclerosis (Edwards, 2009; Homan et al., 2010). Moreover, they are highly social animals with a mostly diurnal circadian profile (Lee, 2004), which makes them more appropriate models for the study of the circadian rhythms, its disorders and possible treatments than the exclusively nocturnal mice and rats.

During ageing, degus also develop signs of inflammation at the brain and retinal level as well as cognitive deterioration (van Groen et al., 2011; Inestrosa et al., 2015). Particularly, older degus have been shown to develop molecular hallmarks of Alzheimer's Disease (AD) (Tarragon et al, 2013; Inestrosa et al., 2005; van Groen et al., 2011; Ardiles et al., 2012, Cisternas et al., 2018). Although the proportion of affected animals still a subject of debate (Steffen et al., 2016; Bourdenx et al., 2017; Hurley et al., 2018), there is very strong evidence for the presence of these symptoms, which is further reinforced by the fact that the aforementioned disorders commonly found in degus (diabetes, circadian disruption, atherosclerosis etc.) are usually comorbid with AD, and frequently considered risk factors for the development of the disease (i.e. Musiek et al., 2015; De Reuck et al., 2016; Ribe and Lovestone, 2016).

Due to their diurnal and social nature, degus are good candidates for models in the study of the melanopsin system. Photoreception in mammals is not limited to conscious visual perception, but also comprises a range of “non-image forming responses” (NIFRs) that include,

Abbreviations: PLR, Pupillary light reflex; ipRGC, Intrinsically-photosensitive reti-nal ganglion cells; PIPR, Post-illumination pupillary response

* Corresponding author.
E-mail address: nicolas.palanca@cinv.cl (N. Palanca-Castan).

https://doi.org/10.1016/j.exer.2019.107866
Received 24 June 2019; Received in revised form 6 September 2019; Accepted 28 October 2019
Available online 02 November 2019
0014-4835/

among others, the regulation of circadian rhythms in response to changes in day length and the pupillary light reflex (PLR) or constriction of the pupil when exposed to light (Hatori and Panda, 2010). Non-image forming responses are driven by a small set of intrinsecally photosensitive ganglion cells (ipRGCs), which, unlike the great majority of Retinal Ganglion Cells (RGCs), contain a visual pigment named melanopsin, more similar in structure to invertebrate rhodopsins than to vertebrate opsins, that makes them directly photosensitive (Provencio et al., 2000). . Although rods and cones send signals and influence the responses of ipRGCs, the latter are essential for PLR function (Güler et al., 2008; Hatori et al., 2008). Therefore, ipRGC deterioration will always result in PLR malfunction, regardless of the health of rods, cones or other RGCs. Direct photoreception from ipRGCs is profoundly involved in NIFR. Melanopsin-positive ipRGCs have been shown to project to the suprachiasmatic nucleus (SCN) and the olivary pretectal nucleus (OPN) (Hattar et al., 2006) which are responsible for the regulation of circadian rhythms and pupillary constriction respectively. Studies with genetically modified mice showed that in animals with no rods or cones ipRGCs are sufficient for pupillary constriction (Zhu et al., 2007). Previous studies had shown that rodless, coneless mice that were otherwise blind could still show circadian entrainment when exposed to light pulses (Foster et al., 1991), which we now know was due to the melanopsin system remaining intact in those animals.

In recent years the role of the melanopsin system for human health has started to be better understood. For example, long-term disruption of the circadian system has been found to be a risk factor for several diseases like psychiatric disorders, cognitive and gastrointestinal alterations, obesity, diabetes and breast cancer (Hatori et al., 2017). In addition, not only are spontaneous disruptions of the circadian rhythm considered symptomatic of Alzheimer's disease (AD), but it has been suggested that circadian dysfunction precedes symptom onset, as it has been shown that adequate sleep has a neuroprotective effect against the deposition of amyloid plaques that is lost in the presence of extended circadian disruption (Musiek et al., 2015). Moreover, some findings suggest that AD selectively affects the melanopsin system (La Morgia et al., 2016): retinas of AD patients were found to have suffered ipRCG loss even when RGC count was normal, with remaining ipRGCs showing signs of deterioration and amyloid pathology. The association between the melanopsin system and neurodegenerative diseases has been recently been explored in several studies, which has led to the consideration of the retina as a biomarker and a target for methods of early diagnosis (Meltzer et al., 2017; La Morgia et al., 2017).

In this context, *O. degus* emerges as an informative model for the study of the melanopsin system. From the point of view of basic science, its mostly diurnal behavior and his phylogenetic position as a rodent make it a good candidate for comparative studies that aim to find out the relationships between circadian behavior and the melanopsin system. Its diurnal behavior also makes them more similar to humans than standard rodent models, and a preliminary study of their melanopsin amino acid sequence finds more similarities between degu and human melanopsin than between degus and mice/rats (Fig. 1), which could indicate some degree of convergence based on behavioral and ecological constraints. From the point of view of applied science, as mentioned above, degus suffer many of the diseases connected to the deterioration of the melanopsin system, including AD and general age-related neurodegeneration, which makes them valuable for biomedical studies.

As part of biomedical studies involving a new animal model, it becomes important to develop tools that can be easily used to detect and observe the appearance and progression of early symptoms of disease, so that animals suffering them can be subject to further tests or be put in observation. The present study deals with the development and application of a method for the measurement of the pupillary light reflex in wake *O. degus*. It represents a first approach to a characterization of the pupillary light reflex in *O. degus*, and establishes a quick, affordable method to evaluate the general retinal health and the specific function of the melanopsin system, opening the way for more in-depth and longitudinal studies of our experimental population.

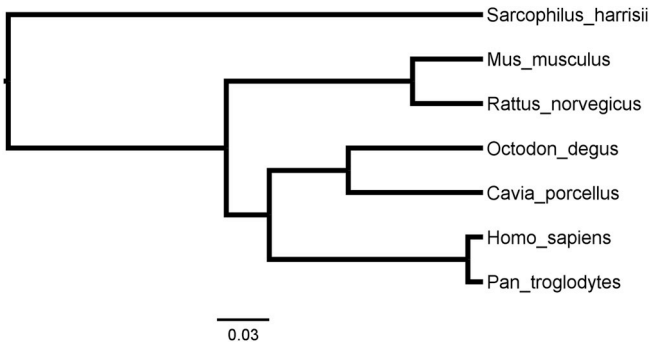

Fig. 1. Phylogenetic tree of melanopsin using amino acid sequences obtained from the NCBI database. The species use and the accession numbers for their sequences were: tasmanian devil (*Sarcophilus harrisii*, XP_003754961.1), guinea pig (*Cavia porcellus*, XP_003466192.2), degu (*Octodon degus*, XP_012372369.2), chimpanzee (*Pan troglodytes*, XP_016774287.1), human (*Homo sapiens*, AAF24978.1), rat (*Rattus norvegicus*, NP_620215.1) and mouse (*Mus musculus*, AAF24979.1). A multiple alignment was performed with Clustal Omega, and the trees were constructed via a Monte Carlo Markov Chain method using the BEAST software (v1.10.4) package and visualized using FigTree (v1.4.4).

2. Methods

2.1. Animals

Our individuals tested were 12 adult individuals of *Octodon degus* (4 males, 8 females), of ages between 6 and 48 months. Two additional animals from concurrent experiments were also tested and used for histology. Information for our study animals can be found in Table 1 All animals were kept at the animal facility of the Facultad de Ciencias from Universidad de Valparaiso as part of an experimental colony used in several projects. The treatment and manipulation of animals followed the rules and guidelines set by the bioethics committee of Universidad de Valparaiso, and the experiments were performed with their previous approval.

2.2. Pupillary light reflex setup

The experimental setup consisted on a heating blanket affixed to the table and marked in order for the animal's position to be reproducible. On one side of the animal was a fixed optical fiber with a diffusing lens affixed on one end, while the other was fitted with a coupling specifically designed to fit with the LED lights used on our experiments.

Table 1
Detailed list of the animals used in our experiments.

ID	Sex	Date of birth	Pupillometry					PLR
			390	450	500	525	605	
000796BD77	Female	12/03/2015	Yes	Yes	Yes	Yes	Yes	PLR-
000796D3C7	Female	19/04/2015		Yes	Yes	Yes	Yes	PLR+
000796C043	Female	07/06/2015	Yes	Yes	Yes	Yes	Yes	PLR-
000796BD54	Female	07/06/2015		Yes	Yes	Yes	Yes	PLR-
000796BFFE	Female	29/08/2016		Yes	Yes	Yes	Yes	PLR-
000796E70C	Female	29/08/2016	Yes	Yes	Yes	Yes	Yes	PLR+
0007AC2E84	Female	08/09/2017	Yes	Yes	Yes	Yes	Yes	PLR+
0007AC6794	Male	08/09/2017	Yes	Yes	Yes	Yes	Yes	PLR+
0007ABC032	Female	08/09/2017		Yes	Yes	Yes	Yes	PLR+
0007ABF2EF	Male	09/10/2017		Yes	Yes	Yes	Yes	PLR-
0007AC3C19	Male	09/10/2017	Yes	Yes	Yes	Yes	Yes	PLR-
000796B287	Female	26/11/2012		Yes		Yes		PLR-
000796C49F	Female	27/09/2014		Yes		Yes		PLR-

Stimuli were generated with a custom-made lamp, consisting on a ring of LED lights connected to an Arduino processor, which allowed, via custom software, to select the LED light to be turned on, its intensity, the duration of the pulse and the duration of the inter pulse interval. For each stimulus, the correct LED was coupled to the optical fiber, and the diffusing lens helped to illuminate the eye of the animal homogenously. A high-definition webcam was used to record the eye contralateral to the stimulus and the time-course of the consensual pupillary light reflex at 30 frames per second.

2.3. Experimental protocol

The stimulus intensity was calibrated before every experiment using a Newport 1918-R power meter (Newport Corporation, CA, USA), and the stimulation was set such that a full power LED illuminated the eye with an intensity of 90 mW/cm^2. Animals were dark-adapted for at least 1 h before the experiments. Previous to every series of stimuli, they were handled gently for around 15 min until they were relaxed and accustomed to their environment and their researchers. Each series consisted on a series of 1-s pulses followed by 15-s interstimulus intervals, and the whole series was recorded together. Each of the examined wavelengths was tested on a separate session for each degu, and during each session we tested intensities at 18, 36, 48, 72 and 90 mW/cm^2 of LED intensity. Intensities were tested in ascending order with breaks of 10 min in darkness between each series of pulses to minimize the effects of habituation. The first experimental series in all tested degus was a first approach to the method and consisted in series of 10 pulses in which only 100% intensity was tested. Only 470 and 500 nm were tested this way. As the results from this first experimental series were consistent between pulses, we tried to optimize the procedure by using 3 pulses in the latter series. Inter-pulse variability, measured as standard deviation, was not significantly different between series 10-pulse and 3-pulse series at 100% intensity (Mann-Whitney U test, $p = 0.974$). Inter-pulse variability was also not dependent on intensity (Kruskal-Wallis h test, $p = 0.066$), and the inter-pulse variability of responses to 100% intensity did not show significant differences with responses to lower intensity pulses (Mann-Whitney-U, $p = 0.110$). Given these results, only 3 pulses were used for the remainder of the experiments.

Pulses at 100% intensity were not consistently different to those that were done in isolation and those done as part of ascending intensity series, indicating that the effects of habituation were negligible. As other rodents, degus are known to have short-wavelength cones with maximum sensitivity within the ultraviolet spectrum, therefore, we also aimed to characterize the PLR in response to UV light using a 390 nm LED. The procedure was similar to the other tests, but in order to avoid any damage to the animal's eyes, we used lower intensities (6, 12 and 18 mW/cm^2).

2.4. Video analysis

Recordings were split into separate frames using Free Video to JPG Converter (DVDVideoSoft Ltd., United Kingdom) and analyzed using a custom Matlab script. As *Octodon degus* has an elliptical vertical pupil rather than the circular shape found in rats, mice, and humans, previously available scripts proved unreliable, and we created our own. The first step of the analysis was to select a set of frames corresponding to a single stimulus, comprising the frames from the start of the light pulse to the one immediately preceding the next pulse, plus fifteen frames just prior to the stimulus that were used to determine the resting size of the pupil. Therefore, the total duration of each measurement was 16.5 s, 0.5 for the baseline, 1 for the stimulus and 15 for the interstimulus interval. Analyzed frames were converted to gray scale by the script. The pupil was measured using three user-defined parameters: a starting point within the pupil, a color *threshold* that defined the minimum darkness that the program would accept in a pixel to be considered a part of the pupil, and a number of *strikes*, which defined the maximum number of pixels above threshold that would be accepted by the program before considering that the edge of the pupil had been reached. The *strikes* variable was there to keep reflections or hairs within the pupil area from causing errors in measurement and could be adapted to ignore these small obstacles. The program then, using the user-defined point as a start, examined pixels to the right, left, up and down separately, counting a strike whenever the pixel color was lighter than the threshold; whenever the program found a number of consecutive strikes larger than the *strikes* variable, the edge of the pupil was set to the pixel n positions before the current one, where $n = strikes$. In order to compensate for uneven conditions in the recording or eye shape, the script can be easily modified so that *threshold* and *strikes* are set independently for up, down, left and right. In addition, the script contains the option to use the *histeq* function in order to enhance the contrast of each frame.

Given that these tests are performed without anesthetics or restriction devices, small head movements were frequent in our recordings, the most common of which were small vertical movements associated with breathing. This proved problematic, as due to the shape of the pupil, small head movements could cause the measurement to occur at different points in the pupil, which would drastically change the result. Due to this, the vertical line was established as reference rather than a measurement. Vertical *threshold* and *strikes* values were optimized for stability, which sometimes implied making them permissive enough for the vertical measurement to include the whole eye rather than the pupil. The horizontal measurement was then stabilized using the vertical measurement as reference; the starting point for each frame from the second onward was recalculated based on the relative point at which the horizontal measurement crossed the vertical measurement on the previous frame. This prevented us from using the vertical measurement to calculate pupil area but gave us a more stable and consistent horizontal measurement, which we prioritized. On those occasions were both measurements were available, area was calculated and found to correlate very well with horizontal diameter. The resting size of the pupil was determined separately for each pulse by averaging the 15 frames (0.5 s) immediately prior to the light pulse. The absolute horizontal pupil diameter in pixels was then determined for each frame separately and normalized to a percentage of the resting size. The normalized horizontal pupil diameter will be referred from now on as "pupil size" for the sake of brevity.

2.5. Data processing

Once the time-series of the PLR was extracted, we determined the maximum constriction and the latency from the stimulus as the baseline measures for the different wavelengths and intensities. The lineal part of the power-response curve for each wavelength was identified and a linear fit was used to characterize its general trend. Immediate subsaturation intensities were identified and were the focus of the analysis, as they are strong and consistent enough to be reliable for the analysis without being affected by adaptation.

To further determine the spectral sensitivity of degu PLR, we used a method similar to that of Gamlin et al. (2007). Briefly, we fitted the irradiance-response PLR data with the Hill Equation:

$$Constriction = Pmax * [I^B/(I^B + C^B)]$$

where I equals irradiance, Pmax represents maximum pupillary constriction and C represents the irradiance at which constriction equals half the maximum. B is a constant that defines the slope of the curve. These curves were found separately for each wavelength and used to determine the quantal sensitivity of the PLR as a function of wavelength. We then compared our data with known absorbance bands of several pigments (Stavenga et al., 1993) and found the best correspondence.

Constriction speed was calculated as the maximum pupillary

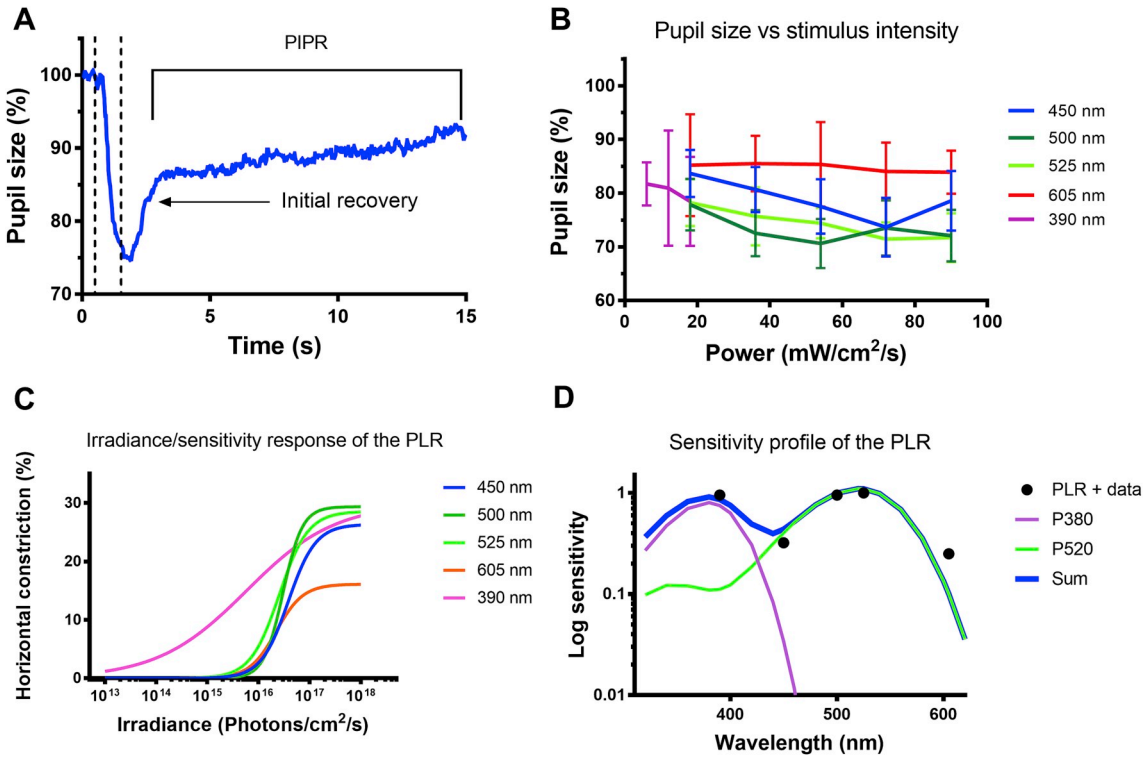

Fig. 2. Pupil constriction at different wavelengths and intensities in PLR + degus. A) A representative PLR response to a subsaturation stimulus of 450 nm. The X axis represents time of the recording in seconds, and the y axis represents the normalized horizontal diameter of the pupil. Dashed lines mark stimulus onset and offset. It is important to note the slow pupil size recovery after stimulus offset, the post-illumination pupil response (PIPR). **B)** Average pupillary constriction of our benchmark animals in response to the different stimulus intensities used. The X axis represents the power of the stimulus in mW/cm^2, while the Y axis represents the average maximum horizontal constriction of our benchmark animals in response to that stimulus. Error bars represent the standard deviation of the mean. Each separate line represents one of our stimulus wavelengths, violet: 390 nm dark blue: 450 nm, green: 500 nm, yellow: 525 nm and red: 605 nm. **C):** Irradiance-sensitivity curves obtained by fitting Hill Equations to our data, the X axis shows irradiance in photons/cm^2/s, while the Y axis shows normalized horizontal constriction in percentage. Each separate line represents one of our stimulus wavelengths, violet: 390 nm dark blue: 450 nm, green: 500 nm, yellow: 525 nm and red: 605 nm. D) Estimation of the degu PLR spectral sensitivity profile from our data. The X axis represents wavelength in nm, The Y axis represents log sensitivity. Black dots mark our data, the violet and green lines represent the spectral sensitivity of visual pigments with maximum sensitivity at 480 and 520 nm, respectively. The blue thick line represents the sum of both sensitivity spectra.

constriction divided by the time in seconds from the stimulus. Pupil size rarely returned to the basal state within the recording time, and we used this "residual constriction" as one of our parameters, calculated as the average pupil constriction from 5 s after the stimulus to the end of the recording. Residual constriction was then used to calculate redilation speed; briefly, constriction values were examined frame by frame after the stimulus and compared with the residual constriction calculated for that recording, and after a previously decided number of frames with constriction under threshold, an end point was set. The constriction difference between the end point and the maximum constriction was divided between the time elapsed in seconds in order to calculate redilation speed. A further characterization of the time course was performed to measure the persistence of post-stimulus pupillary response (PIPR). The average constriction during each second of recording was calculated for sub-saturation responses at all wavelengths to identify those stimuli that elicited a more persistent constriction and were likely to serve as biomarkers of iPRGC function. Fig. 2A shows an example of a typical pupillary light reflex, including the slow redilation that characterizes the PIPR.

2.6. Index rating

To test our animals, we determined a benchmark against which the PLR of our test animals could be compared. To do this, we calculated the average responses of all our characterized individuals to every combination of wavelength and intensity, as well as their standard deviation. Then, for each individual animal, we compared the maximum constriction in response to each stimulus with the averaged maximum constriction from the whole population. Responses that were smaller than the average minus one standard deviation were considered "deteriorated" for that specific stimulus. Only animals that with no deteriorated responses to any combination of wavelength + intensity were selected as "benchmark animals" (PLR + for short) and considered representatives of a healthy population, while the rest were considered to have some degree of deterioration, and will be referred to as PLR-. In this paper we used the PLR + animals to characterize the main differences between healthy and deteriorated animals.

2.7. Statistical methods

Responses of PLR + and PLR- degus were pooled across groups. The maximum constriction of both groups was compared for each combination of frequency and intensity using nonparametric methods (Mann-Whitney *U* test). For the second-by-second responses used to characterize the PIPR, all the raw responses were taken for each combination of PLR, wavelength, and the average constriction and standard deviation were calculated for each time slice. For each combination of time slice, intensity and wavelength, Mann-Whitney *U* tests were conducted between PLR + and PLR- responses.

To test for the effect of age on the PLR, the maximum response for each pulse was calculated as above, responses were pooled for each animal and combination of intensity and wavelength. Firstly, responses were grouped according to degu age, and a Kruskal-Wallis test was performed examining the overall effect of age on the PLR. In addition, a

second test was performed where animals were broadly classified in "young" and "aged" groups, considering the cutoff at 24 months. A Mann-Whitney *U* test was used to determine the presence or absence of significant differences in PLR between groups.

2.8. Immunostaining

Experimental animals (two PLR- degus, 36 and 48 months old and a 36-month old PLR+ animal) were anesthetized with 3.5% isoflurane and decapitated after loss of the toe-pinch reflex. Isolated retinas were fixed in 4% paraformaldehyde during 1 h at 4 °C and rinsed with PBS 1x. Retinal cryostat sections of 18 mm were incubated using a blocking solution (0.2% gelatin/1% Triton X-100 in PBS) during 1 h at room temperature and then stained against primary antibodies [mouse anti-GFAP conjugated with Alexa 488 (1:300) and rat anti-CD11b (1:250), both from BD Biosciences, prepared in blocking solution supplemented with 10% NGS], during 3 h at room temperature. Secondary antibody Alexa 488 (1:250), also prepared in blocking solution with 10% NGS, was incubated at room temperature during 45 min. After several PBS 1x washes, samples were stained with DAPI (25 μM) for 10 min and mounted with Fluoromont G. Neuronal death was assessed using Fluoro-Jade C (0.0001%) for 30 min, as recommended (Merck Millipore), co-incubated with DAPI (25 μM) and mounted with Fluoromont G. For image acquisition, a Nikon C1 Plus confocal microscopy (financed by MECESUP grant UVA0805) was used.

3. Results

Of the 11 animals we tested, 5 of them had responses within our standards to every stimulus and were classified as PLR+, while the other 6 were considered PLR-. Table 1 shows information on each of the degus used for this study. Regardless of age, animals were healthy and no abnormal behaviors were noticed. We selected animals with no obvious signs of obesity or vision deficiencies (e.g. cataracts).

Fig. 2B shows the responses to each power level and wavelength of our benchmark degu population. In general, responses followed generally a linear trend until 80 percent LED power (72 mW/cm^2), after which the responses stabilized or declined due to adaptation and persistent pupil constriction. An exception was the response to 500 nm, which saturated earlier, at 40 percent LED power (36 mW/cm^2), marking it as the wavelength of highest sensitivity for the degu PLR. Response latency showed a general downwards trend with power for all wavelengths in benchmark animals but showed an overall very high variability. Redilation speed was also highly variable, and thus presented no significant differences between stimulus types or intensities. Fig. 2C shows the best-fitting Hill Equations to our data for each of our tested wavelengths. The spectral sensitivity curve derived from our data best fits a combination of photoreceptor pigments at 380 and 520 nm (2D).

As a trend, 450 nm elicited the largest residual constriction. Subsaturation residual constrictions elicited by 500 and 525 nm were similar, while 605 elicited the smallest. Figs. 3 and 4 show the PIPR for all animals, conditions, wavelengths and intensities, represented as an average of the second-to second response. The PIPR showed a significant effect of wavelength used, with 450 nm eliciting a more persistent response that other wavelengths at the immediate sub-threshold intensity. Responses elicited by 500 and 525 nm showed a similar degree of persistence, while 605 was the least persistent. The data for the UV pupillometry showed increasing constriction with intensity, and its maximum constriction was similar to that of the response to 500 nm at the intensity where measurements overlapped, indicating a similar degree of sensitivity.

When comparing degus of different ages, there was a significant effect of age on the PLR response in 2 out of 20 combinations of intensity and wavelength (Kruskal-Wallis *h*-test, $p < 0.05$. For the full values see Supplementary Table 1). When dividing degus in two groups, young (< 24 months) and aged (> 24 months), there were significant differences between the responses of the two groups in 3 out of 20 combinations of intensity and wavelength (Mann-Whitney *U* test, $p < 0.05$. For the full values see Supplementary Table 2).

When comparing PLR+ and PLR- animals, pupillary responses were significantly larger in benchmark animals for 19 out of 20 combinations of intensity and wavelength (Mann-Whitney *U* test, $p < 0.05$, Supplementary Table 2), the exception being 450 nm at 48 mW/cm^2 (Mann-Whitney *U* test, $p = 0.093$, Supplementary Table 3). Side-by-side comparisons of the second-by-second responses of PLR+ and PLR- animals can be found in Figs. 3 and 4. To further characterize the responses and find the largest differences between PLR+ and PLR- animals, we subtracted the averaged second-by-second subthreshold responses of PLR- animals from those of PLR+ animals (Fig. 4E). The largest differences were found at the point of maximum constriction, and the magnitude of the differences for each wavelength followed the order of sensitivity found in the general characterization: 500 nm first, followed by525 nm, 450 nm and, lastly, 605 nm. Differences between PLR+ and PLR- animals diminished with time, although the difference elicited by 450 nm showed considerable persistence (Fig. 4F). When examining the differences in the PIPR at 10 s for 450 and 525 nm, 72 mW/cm^2 between PLR+ and PLR- animals, there were clear differences between PLR+ and PLR- animals when stimulated with 450 nm light (Mann-Whitney *U* test, $p = 0.00056$) that were absent when stimulating with 525 nm, a graphic representation of these responses can be seen in Fig. 4E.

The results of our preliminary histological analyses of some degus tested with our method (Fig. 5) show no Fluoro-Jade staining in the examined PLR+ degus, while PLR- showed staining to several degrees in either the retina or the hippocampus. Notably, no PLR- showed staining in both retina and hippocampus.

4. Discussion

We successfully developed an experimental setup and protocol that allowed us to characterize the pupillary light reflex in awake degus and examine their overall sensitivity as well as their response to specific wavelengths. To our knowledge, this is the first time chromatic pupillometry has been used on a diurnal rodent. Literature on the PLR in general is scarce when it comes to diurnal rodents. The most detailed study corresponds to Chang et al. (2017), which evaluated the PLR of guinea pigs with white light from a cell phone LED light. The results from that study show a smaller constriction ratio than seen in our experimental animals, which is surprising considering that the white light should be more effective at eliciting pupil constriction. A similarity with our study is the consistency of constriction within a train of pulses (Chang et al., 2015, Fig. 4). Pupil constriction ratio remains similar even if the baseline has not returned to its original size, suggesting that adaptation is not a large factor, at least for these short experiments.

Thus far, degu visual sensitivity had been characterized via electroretinogram (ERG) (Chávez et al., 2003). Our results are generally in agreement regarding the sensitivity peak in the low 500 nm, corresponding to the middle wavelength cones (Fig. 5D). Our test had the advantage to also test the sensitivity of the intrinsically-photosensitive retinal ganglion cells, which are not usually examined in ERGs. Sensitivity of ipRGCs has been tested *in vitro* and found to be close to 480 nm (Berson et al., 2002), although behavioral sensitivity has been shown to vary from 447 to 484 nm (Lucas et al., 2014). An interesting characteristic of melanopsin-mediated responses is that they are not affected by bleaching, or at least not to the extent of visual pigments, thus being the main opsin responsible for prolonged pupil constriction, which is absent in animals that have had their melanopsin gene knocked out (Zhu et al., 2007). In our tests, 500 elicited a larger response, and the overall largest constriction of all tested wavelengths at 48 mW/cm2, before the response declined due to response saturation and adaptation. It is worth noting that our sensitivity curves fit optimally to a sum of

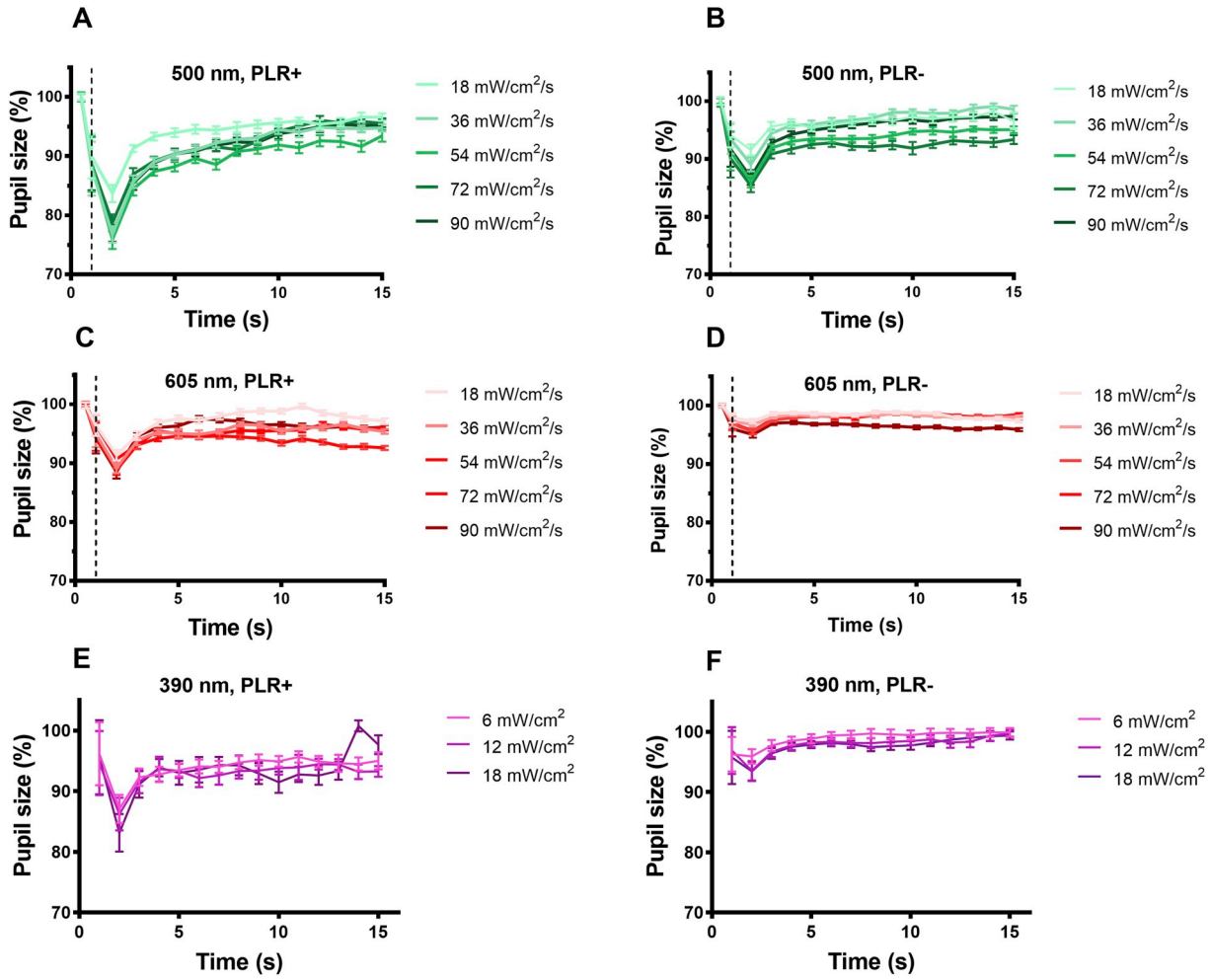

Fig. 3. Decreased pupillary constriction and recovery time at 500, 605 and 390 nm in PLR- animals when compared to PLR + degus. Second-to-second representation of the time course of the responses of PLR+ and PLR- animals to 500, 605 and 390 nm at 18, 36, 54, 72 and 90 mW/cm^2 intensities. Normalized horizontal pupil diameter percentage after X time of light exposition. Each data point represents the averaged response of all PLR during the preceding second, thus, second 1 represents the average response between the 0 and 1 s of the recording, second two the response between seconds 1 and 2 and so on. Error bars represent standard deviation (n = 5). Panels: A) 500 nm, PLR+ animals, B) 500 nm, PLR- animals, C) 605 nm, PLR+ animals, D) 605 nm, PLR- animals, E) 390 nm, PLR + animals, F) 390 nm, PLR- animals.

two visual pigments with maximum sensitivities at 380 and 520 nm (Fig. 2D), rather than the 360 and 500 observed in previous studies (Chávez et al., 2003; Jacobs et al., 2003). However, the methodological differences between such studies make it difficult to determine the significance of this difference. Most notably, our animals were not anesthetized or given atropine, we made a pre-selection for healthy PLR that was absent in other studies and used the pure behavioral data without accounting for any spectral filtering by ocular media.

However, constriction persistence was larger in response 450 nm than to other frequencies. Therefore, 450 nm is, from our tested wavelengths, the most likely to stimulate ipRGCs optimally.

Few studies thus far have measured the PLR in response to ultraviolet (UV) light, despite it being known that rodents have cones that perceive light in the UV spectrum (Yao et al., 2006). For the sake of completeness, we aimed to characterize the PLR response of degus in response to 390 nm. Although we used lower intensities to ensure the well-being of our experimental subjects, we found consistent and sensitive responses in our benchmark degus. At the intensity where both UV and other wavelengths were measured, the response to 390 nm was comparable to the response to 500 nmwhich is in accordance with the results found in mice by Yao and collaborators (2006).

Beyond our basic characterization of the healthy PLR, our test was able to detect significant differences between our benchmark animals and those with some degree of deterioration. The PLR test differentiated PLR+ from PLR- via two main characteristics of the response. The first one, maximum constriction, was common to all tested wavelengths (Fig. 4E). Maximum constriction is therefore a diagnostic character that could be used to separate healthy and deteriorated degus for further experiments and observations. Such a deterioration of the PLR can be caused by wide range of disorders (Hall and Chilcott, 2018). and although a deterioration of the PLR is a hallmark of some degenerative disorders such as Alzheimer's or Parkinson's diseases (e.g. Giza et al., 2011, Micieli et al., 1991), the presence of other possible causes makes it necessary to use some other characters to narrow down the diagnosis.

The second differentiating characteristic of the PLR in the studied animals was the Post-illumination pupillary response (PIPR), which can be defined as a persistent pupillary constriction in response to light. PIPR showed a large difference between PLR+ and PLR- animals in those responses elicited by 450 nm. The response to 450 nm in benchmark animals was larger, and that difference was sustained with little change during the whole of the recording, in contrast to the differences in response elicited by other wavelengths, which declined rapidly after stimulus offset (Fig. 4E).

The persistent pupil constriction of the PIPR is a consequence of the direct stimulation of ipRGCs by light within the melanopsin sensitivity range (Gamlin et al., 2007). Therefore, deficiencies in the PIPR can be

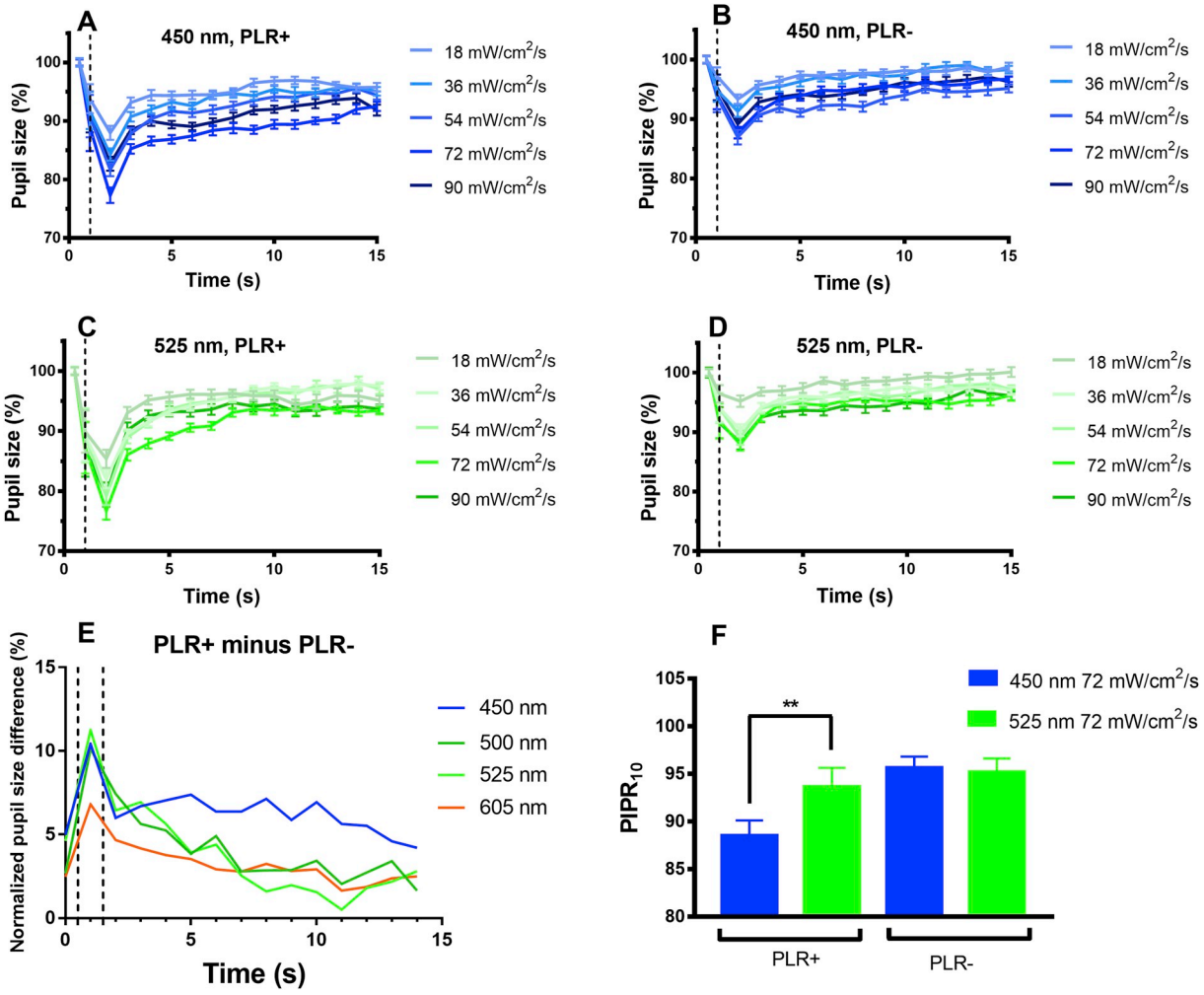

Fig. 4. Decreased pupillary constriction and recovery time at 450 and 525 nm in PLR- animals when compared to PLR + degus Panels A-C: Second-to-second representation of the time course of the responses of PLR + and PLR- animals to 450 and 525 nm at all tested intensities. The X axis represents the time of the recording in seconds, and the Y axis represents the normalized horizontal diameter of the pupil in percentage. Each line represents one of the intensities (18, 36, 54, 72 and 90 mW/cm^2), represented by darker lines for higher intensities. Each data point represents the averaged response of all PLR or PLR- during the preceding second, thus, second 1 represents the average response between the 0 and 1 s of the recording, second two the response between seconds 1 and 2 and so on. Error bars represent the standard deviation of the mean. A) 450 nm, PLR + animals, B) 450 nm, PLR- animals, C) 525 nm, PLR + animals, D) 525 nm, PLR-. Panel E: Subtraction of the PLR + minus the PLR-time courses. The X axis shows the time of the recording in seconds. The Y axis represents the difference between the average responses of PLR + and PLR- animals for each given second of the recording, expressed in percentage of the pupil resting size. Vertical dashed lines represent the onset and offset of the stimulus. **Panel F:** Comparison between the average PIPR of PLR + and PLR- animals in response to subsaturating stimuli at 450 and 525 nm, during seconds 9–10 of the recording. Blue bars represent responses to 450 nm and 72 mW/cm^2, while yellow bars represent responses to 525 nm and 72 mW/cm^2. The two bars to the left represent the response of PLR + animals, and the 2 bars to the right, the response of PLR- animals. The Y axis represent the average normalized horizontal diameter during second 9–10 of the recording (PIPR$_{10}$). Error bars represent standard deviation. The PIPR$_{10}$ values for 450 and 525 nm of PLR + animals were significantly different (denoted by two asterisks).

considered to arise from a specific deterioration of the melanopsin system. The use of chromatic pupillometry to isolate and measure the part of the response that corresponds to the stimulation of melanopsin has been suggested before as a tool to identify retinal neuropathies in humans (Feigl et al., 2012; Meltzer et al., 2017; Hall and Chilcott, 2018). For our own analysis, we used a similar paradigm to Park et al. (2011), where we measured the contrast between the response to a stimulus within the sensitivity range of melanopsin and another outside of it. In human studies these two stimuli are blue and red. However, degus do not have cones tuned to the red part of the spectrum, so instead we used 525 nm, which was well away from our melanopsin stimulus (450 nm) yet elicited a response of similar amplitude at similar intensities. The result of comparing the PIPR in response to subsaturating stimuli at 450 and 525 nm can be seen in Fig. 4E. In our data, the difference in the PIPR in PLR + animals peaked between seconds 9 and 10 of the recording, a difference that was absent in PLR- individuals. This value, that can be abbreviated as PIPR$_{10}$, has potential as a biomarker to screen animals for deficiencies in ipRGC function. Animals that show deterioration can then be subjected to more specific methods in order to determine whether they are suffering from neurodegeneration.

It is important to note that, although our test detected significant differences between older and younger degus for some of the stimuli used, those differences were only found in 3 of 20 stimulus variants, while we detected significant differences in 19 of 20 stimulus variants between PLR + and PLR- animals. Moreover, both age groups contained PLR + and PLR- animals. Therefore, although it is to be expected that deterioration will be more common in older animals, this pupillometry test is not detecting a general age-related deterioration, but some disorder that can appear independently of age.

The purpose of this test is to screen animals of all ages and with no obvious diseases, with the intention of being able to detect those in the

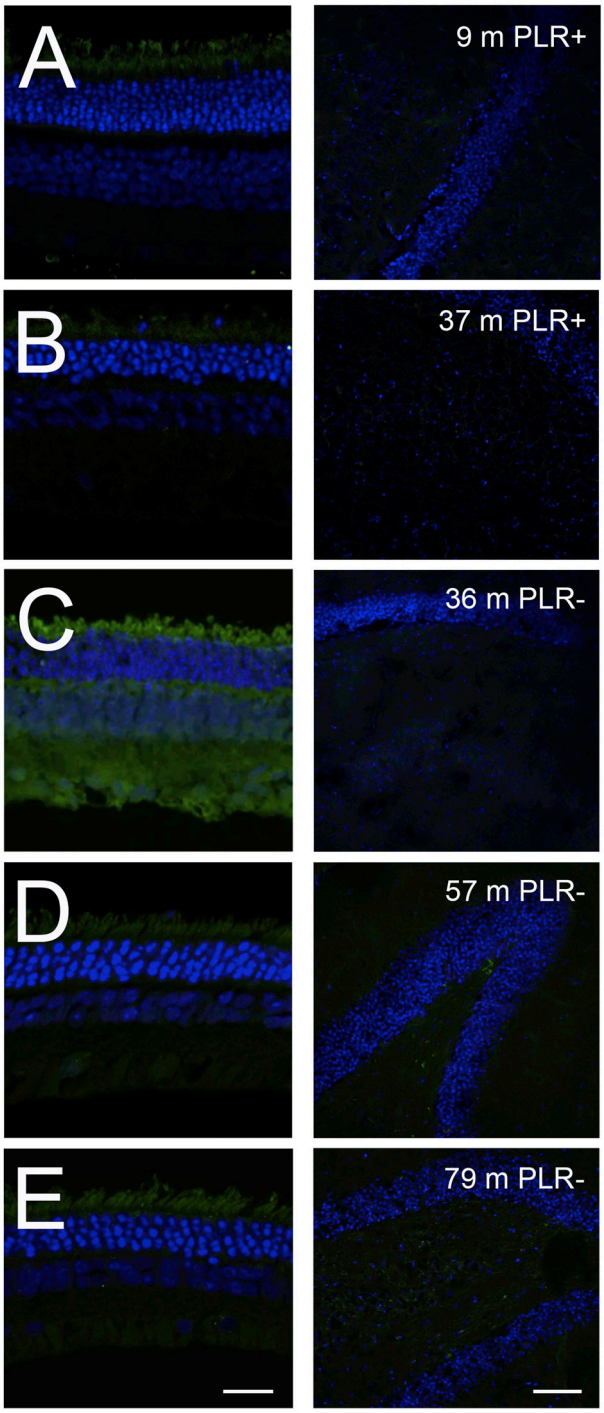

Fig. 5. Increased neuronal death marker expression in retinas from PLR- degus. Representative immunostaining from retina (left) and hippocampus (right) of some degus tested with our method. Each row represents a different degu: 9 m PLR+ (A), 37 m PLR+ (B), 36 m PLR- (C), 57 m PLR- (D) and 79 m PLR- (E).

first stages of deterioration. For this reason, we separated as PLR + those degus with the absolute best sensitivity to create a benchmark. Our intention is to use a very strict standard as we start screening our colony, as we would rather our test created false positives than leave deteriorated animals unnoticed. Therefore, in future studies we will consider as PLR- any animal that presents either maximum constriction or $PIPR_{10}$ below the average of our PLR+ animals minus one standard deviation. Were we to find a large number of false positives, the test parameters can be relaxed to average minus two standard deviations, more in line with usual conventions.

In conclusion, we were able to develop a non-invasive and affordable method for carrying out chromatic pupillometry in awake degus and performed the first characterization of the pupillary light reflex on this animal. Moreover, we developed a protocol to classify our animals according to PLR performance, which gives us an easy way to screen our colony for animals showing potential ipRGC dysfunction. Although selective deterioration of ipRGCs is suggested to be present in AD, and chromatic pupillometry is considered a promising diagnostic method (Chougule et al., 2019), it is as yet unknown how consistent is ipRGC loss, especially at earlier stages in the disease. Another complicating factor is that some other conditions, like glaucoma, can result in melanopsin cell dysfunction (Kankipati et al., 2011). Our preliminary histological study of animals evaluated using our methods found signs of neuronal cell death in either the retina or the hippocampus of PLR- animals, while PLR+ animals showed no such signs. However, PLR- animals never showed cell death consistently in retina, hippocampus or both. Due to the low number of sacrificed animals since the method was implemented, we have been unable to assess whether neurodegeneration in retina and hippocampus affects PLR deterioration in different ways. Future studies will continue to test the strength of the relationship between a deteriorated PLR and the presence of neurodegenerative disorders, and the specificity of diagnosis that can be achieved using different PLR characteristics. Although much work remains to be done, we consider the development and implementation of our chromatic pupillometry test a promising advance towards the establishment of *O. degus* as a more standardized animal model for comparative and biomedical studies.

Acknowledgements

FONDECYT postdoctoral 3180149. Millennium Institute P029-022, Chile. Confocal microscopy financed by MECESUP UVA0805

Appendix A. Supplementary data

Supplementary data to this article can be found online at https://doi.org/10.1016/j.exer.2019.107866.

References

Ardiles, Á.O., Tapia-Rojas, C.C., Mandal, M., Alexandre, F., Kirkwood, A., Inestrosa, N.C., Palacios, A.G., 2012. Postsynaptic dysfunction is associated with spatial and object recognition memory loss in a natural model of Alzheimer's disease. Proc. Natl. Acad. Sci. 109 (34), 13835–13840.

Ardiles, A.O., Ewer, J., Acosta, M.L., Kirkwood, A., Martinez, A.D., Ebensperger, L.A., et al., 2013. *Octodon degus* (Molina 1782): a model in comparative biology and biomedicine. Cold Spring Harb. Protoc. 4, 312–318. https://doi.org/10.1101/pdb.emo071357.

Berson, D.M., Dunn, F.A., Takao, M., 2002. Phototransduction by retinal ganglion cells that set the circadian clock. Science 295 (5557), 1070–1073.

Bourdenx, M., Dovero, S., Thiolat, M.L., Bezard, E., Dehay, B., 2017. Lack of spontaneous age-related brain pathology in Octodon degus: a reappraisal of the model. Sci. Rep. 7, 45831.

Chang, A.M., Aeschbach, D., Duffy, J.F., Czeisler, C.A., 2015. Evening use of light-emitting eReaders negatively affects sleep, circadian timing, and next-morning alertness. Proc. Natl. Acad. Sci. 112 (4), 1232–1237.

Chang, L.Y.L., Turuwhenua, J., Qu, T.Y., Black, J.M., Acosta, M.L., 2017. Infrared video pupillography coupled with smart phone LED for measurement of pupillary light reflex. Front. Integr. Neurosci. 11, 6.

Chávez, A.E., Bozinovic, F., Peichl, L., Palacios, A.G., 2003. Retinal spectral sensitivity, fur coloration, and urine reflectance in the genus Octodon (Rodentia): Implications for visual ecology. Investig. Ophthalmol. Vis. Sci. 44 (5), 2290–2296.

Chougule, P.S., Najjar, R.P., Finkelstein, M.T., Kandiah, N., Milea, D., 2019. Light-Induced pupillary responses in Alzheimer's disease. Front. Neurol. 10.

Cisternas, P., Zolezzi, J.M., Lindsay, C., Rivera, D.S., Martinez, A., Bozinovic, F., Inestrosa, N.C., 2018. New insights into the spontaneous human Alzheimer's disease-like model Octodon degus: unraveling amyloid-β peptide aggregation and age-related amyloid pathology. J. Alzheimer's Dis. 1–19 (Preprint).

De Reuck, J., Deramecourt, V., Cordonnier, C., Pasquier, F., Leys, D., Maurage, C.A., Bordet, R., 2016. The incidence of post-mortem neurodegenerative and cerebrovascular pathology in mixed dementia. J. Neurol. Sci. 366, 164–166.

Edwards, M.S., 2009. Nutrition and behavior of degus (*Octodon degus*). Vet. Clin. N. Am. Exot. Anim. Pract. 12 (2), 237–253.
Feigl, B., Zele, A.J., Fader, S.M., et al., 2012. The post-illumination pupil response of melanopsin expressing intrinsically photosensitive retinal ganglion cells in diabetes. Acta Ophthalmol. 90 (3), e230–e234.
Foster, R.G., Provencio, I., Hudson, D., Fiske, S., De Grip, W., Menaker, M., 1991. Circadian photoreception in the retinally degenerate mouse (rd/rd). J. Comp. Physiol. 169 (1), 39–50.
Gamlin, P.D., McDougal, D.H., Pokorny, J., Smith, V.C., Yau, K.W., Dacey, D.M., 2007. Human and macaque pupil responses driven by melanopsin-containing retinal ganglion cells. Vis. Res. 47 (7), 946–954.
Giza, E., Fotiou, D., Bostantjopoulou, S., Katsarou, Z., Karlovasitou, A., 2011. Pupil light reflex in Parkinson's disease: evaluation with pupillometry. Int. J. Neurosci. 121 (1), 37–43.
Güler, A.D., Ecker, J.L., Lall, G.S., Haq, S., Altimus, C.M., Liao, H.W., et al., 2008. Melanopsin cells are the principal conduits for rod–cone input to non-image-forming vision. Nature 453 (7191), 102.
Hall, C., Chilcott, R., 2018. Eyeing up the future of the pupillary light reflex in neurodiagnostics. Diagnostics 8 (1), 19.
Hatori, M., Panda, S., 2010. The emerging roles of melanopsin in behavioral adaptation to light. Trends Mol. Med. 16 (10), 435–446.
Hatori, M., Le, H., Vollmers, C., Keding, S.R., Tanaka, N., Schmedt, C., et al., 2008. Inducible ablation of melanopsin-expressing retinal ganglion cells reveals their central role in non-image forming visual responses. PLoS One 3 (6), e2451.
Hatori, M., Gronfier, C., Van Gelder, R.N., Bernstein, P.S., Carreras, J., Panda, S., et al., 2017. Global rise of potential health hazards caused by blue light-induced circadian disruption in modern aging societies. Nat. Partn. J.: Aging Mech. Dis. 3.
Hattar, S., Kumar, M., Park, A., Tong, P., Tung, J., Yau, K.W., Berson, D.M., 2006. Central projections of melanopsin-expressing retinal ganglion cells in the mouse. J. Comp. Neurol. 497 (3), 326–349.
Homan, R., Hanselman, J.C., Bak-Mueller, S., Washburn, M., Lester, P., Jensen, H.E., et al., 2010. Atherosclerosis in *Octodon degus* (degu) as a model for human disease. Atherosclerosis 212 (1), 48–54.
Hurley, M.J., Deacon, R.M., Beyer, K., Ioannou, E., Ibáñez, A., Teeling, J.L., Cogram, P., 2018. The long-lived Octodon degus as a rodent drug discovery model for Alzheimer's and other age-related diseases. Pharmacol. Ther. 188, 36–44.
Inestrosa, N.C., Reyes, A.E., Chacón, M.A., Cerpa, W., Villalón, A., Montiel, J., et al., 2005. Human-like rodent amyloid-β-peptide determines Alzheimer pathology in aged wild-type *Octodon degu*. Neurobiol. Aging 26 (7), 1023–1028.
Inestrosa, N.C., Rios, J.A., Cisternas, P., et al., 2015. Age Progression of Neuropathological Markers in the Brain of the Chilean Rodent *Octodon degus*, a Natural Model of Alzheimer's Disease. Brain Pathol. 25 (6), 679–691.
Jacobs, G.H., Calderone, J.B., Fenwick, J.A., Krogh, K., Williams, G.A., 2003. Visual adaptations in a diurnal rodent, Octodon degus. J. Comp. Physiol. 189 (5), 347–361.
Kankipati, L., Girkin, C.A., Gamlin, P.D., 2011. The Post-Illumination Pupil Response Is Reduced in Glaucoma Patients. Investig. Ophthalmol. Vis. Sci. 52 (5), 2287–2292.
La Morgia, C., Ross-Cisneros, F.N., Koronyo, Y., Hannibal, J., Gallassi, R., Cantalupo, G., et al., 2016. Melanopsin retinal ganglion cell loss in Alzheimer disease. Ann. Neurol. 79 (1), 90–109.
La Morgia, C., Ross-Cisneros, F.N., Sadun, A.A., Carelli, V., 2017. Retinal ganglion cells and circadian rhythms in Alzheimer's disease, Parkinson's disease, and beyond. Front. Neurol. 8, 162.
Lee, T.M., 2004. *Octodon degus*: a diurnal, social, and long-lived rodent. ILAR J. 45 (1), 14–24.
Lucas, R.J., Peirson, S.N., Berson, D.M., et al., 2014. Measuring and using light in the melanopsin age. Trends Neurosci. 37 (1), 1–9.
Meltzer, E., Sguigna, P.V., Subei, A., Beh, S., Kildebeck, E., Conger, D., et al., 2017. Retinal architecture and melanopsin-mediated pupillary response characteristics: a putative pathophysiologic signature for the retino-hypothalamic tract in multiple sclerosis. Jama neurology 74 (5), 574–582.
Micieli, G., Tassorelli, C., Martignoni, E., Pacchetti, C., Bruggi, P., Magri, M., Nappi, G., 1991. Disordered pupil reactivity in Parkinson's disease. Clin. Auton. Res. 1 (1), 55–58.
Musiek, E.S., Xiong, D.D., Holtzman, D.M., 2015. Sleep, circadian rhythms, and the pathogenesis of Alzheimer disease. Exp. Mol. Med. 47 (3), e148.
Park, J.C., Moura, A.L., Raza, A.S., et al., 2011. Toward a clinical protocol for assessing rod, cone, and melanopsin contributions to the human pupil response. Investig. Ophthalmol. Vis. Sci. 52 (9), 6624–6635.
Provencio, I., Rodriguez, I.R., Jiang, G., Hayes, W.P., Moreira, E.F., Rollag, M.D., 2000. A novel human opsin in the inner retina. J. Neurosci. 20 (2), 600–605.
Ribe, E.M., Lovestone, S., 2016. Insulin signalling in Alzheimer' s disease and diabetes: from epidemiology to molecular links. J. Intern. Med. 280 (5), 430–442.
Stavenga, D.G., Smits, R.P., Hoenders, B.J., 1993. Simple exponential functions describing the absorbance bands of visual pigment spectra. Vis. Res. 33 (8), 1011–1017.
Steffen, J., Krohn, M., Paarmann, K., Schwitlick, C., Brüning, T., Marreiros, R., et al., 2016. Revisiting rodent models: *Octodon degus* as Alzheimer's disease model? Acta Neuropathol. Commun. 4 (1), 91.
Tarragon, E., Lopez, D., Estrada, C., Ana, G.C., Schenker, E., Pifferi, F., et al., 2013. *Octodon degus*: a model for the cognitive impairment associated with A lzheimer's disease. CNS Neurosci. Ther. 19 (9), 643–648.
van Groen, T., Kadish, I., Popović, N., Popović, M., Caballero-Bleda, M., Baño-Otálora, B., et al., 2011. Age-related brain pathology in Octodon degu: blood vessel, white matter and Alzheimer-like pathology. Neurobiol. Aging 32 (9), 1651–1661.
Yao, G., Zhang, K., Bellassai, M., Chang, B., Lei, B., 2006. Ultraviolet light–induced and green light–induced transient pupillary light reflex in mice. Curr. Eye Res. 31 (11), 925–933.
Zhu, Y., Tu, D.C., Denner, D., Shane, T., Fitzgerald, C.M., Van Gelder, R.N., 2007. Melanopsin-dependent persistence and photopotentiation of murine pupillary light responses. Investig. Ophthalmol. Vis. Sci. 48 (3), 1268–1275.